ADVANCED MATERIALS
www.advmat.de

Tunable 3D Extended Self-Assembled Gold Metamaterials with Enhanced Light Transmission

*Stefano Salvatore, Angela Demetriadou, Silvia Vignolini, Sang Soon Oh, Sebastian Wuestner, Nataliya A. Yufa, Morgan Stefik, Ulrich Wiesner, Jeremy J. Baumberg, Ortwin Hess, and Ullrich Steiner**

Exploiting self-organised colloids[1,2] and monolayers[3] is a valuable approach to obtaining features at the sub-micrometer scale, but this approach is limited in the achievable architectures and symmetries and consequently in the optical properties that can be realized. Microphase morphologies of polymers, on the other hand, provide a convenient platform for the manufacture of truly three-dimensional metamaterials with a wide range of geometries. In particular the alternating gyroid[4] architecture has received increasing attention[5–10] due to both its continuous 3D structure and chirality. In tailoring the optical response in such metamaterials it is fundamentally important to be able to control their structures and tune their properties. State-of-the-art dynamically tunable infrared metamaterials employ the orientation of a liquid crystalline phase in an ion milled fishnet structure by applying an electric field,[11] but similar systems for optical metamaterials do not yet exist.

In this paper, we tune the optical response at visible frequencies of a bulk metamaterial obtained by replicating a block copolymer self-assembled morphology into Au, using three different tuning methods. In the first, the structural dimensions of the mesoscopic unit cell are controlled by varying the molecular weight of the structure-forming block copolymer. In the two other strategies using post-processing, tuning is achieved by controlling the metal filling fraction of the plasmonic structure or by filling different refractive index media into the metal scaffold. The experimental results show good agreement with finite difference time domain (FDTD) calculations[12] of the full 3D structures and also match an approach based on a three-helix model (THM).[13]

Block copolymers[14] consist of two or more chemically different polymers that are covalently tethered. Self-assembly in such systems is principally driven by enthalpy reduction through microphase separation that minimizes unfavorable interfaces and is balanced by entropic factors encouraging the reduction of chain stretching.[15] Depending on the relative molecular weight and number of blocks, a range of architectures are formed.[16] In this study a polyisoprene-*block*-polystyrene-*block*-polyethylene oxide (ISO) terpolymer,[17,18] which assembles into the alternating gyroid morphology was used as a mold for the fabrication of a plasmonic metamaterial. The block copolymer microphase separates into two interpenetrating, chemically distinct gyroid networks (isoprene and ethylene oxide) embedded in a majority phase (styrene).

The replication of one of the gyroid networks is accomplished by selective degradation and removal of polyisoprene by UV radiation, followed by back-filling of the nanoporous template via the electrodeposition of gold. The remaining polymer is then removed by plasma etching. The optical properties of the resulting gold gyroid were investigated by reflection and transmission spectroscopy in a confocal configuration.

It was shown recently that the nanoplasmonic gyroid's optical properties can be well described by a simplified tri-helical metamaterial (THM) model,[13] assuming that the gyroid's internal structure derives from a network of interconnected metallic helical wires. In particular, there are two types of helices with different radii,[9] the smaller of which determines the optical properties close to the cut-off wavelength (see Figure S4a in the Supporting Information for a 2D representation of the structure). This cut-off wavelength originates from the continuous nature of the metallic helices and is called plasma wavelength. No wave can propagate in the gyroid for wavelengths larger than the plasma wavelength leading to high reflection at these wavelengths. Conversely, there are three propagating modes just below the plasma wavelength which are highly confined within the smaller helices (see Supporting Information, Figure S4b). As a result, the THM model allows us to calculate the plasma wavelength from the following equation which makes use of the geometric parameters of the smaller helices:

$$\lambda_p \approx c_1 a \left\{ \frac{1}{\varepsilon_{Au} f c_2} + \frac{c_3}{\varepsilon_n \left[c_4\sqrt{f} - \sqrt{c_5 + c_6 ln\left(c_7/\sqrt{f}\right)} \right]^2} \right\}^{-\frac{1}{2}} \quad (1)$$

where f and a are the filling fraction and unit cell of the gyroid, ε_n is the dielectric constant of the medium (with refractive index n) the gyroid is immersed in, ε_{Au} is the dispersive permittivity of gold, and c_{1-7} are geometrical coefficients (see Supporting Information). The optical properties can therefore be tailored by varying

S. Salvatore, Dr. S. Vignolini, Dr. N. A. Yufa, Prof. J. J. Baumberg, Prof. U. Steiner
Cavendish Laboratory
Department of Physics
University of Cambridge
J. J. Thomson Avenue, Cambridge CB3 0HE, UK
E-mail: u.steiner@phy.cam.ac.uk
Dr. A. Demetriadou, Dr. S. S. Oh, Dr. S. Wuestner, Prof. O. Hess
Blackett Laboratory
Department of Physics
Imperial College London
South Kensington Campus, London SW7 2AZ, UK
Dr. M. Stefik, Prof. U. Wiesner
Department of Materials Science & Engineering
Cornell University
Ithaca, New York 14853, USA

DOI: 10.1002/adma.201300193

© 2013 WILEY-VCH Verlag GmbH & Co. KGaA, Weinheim

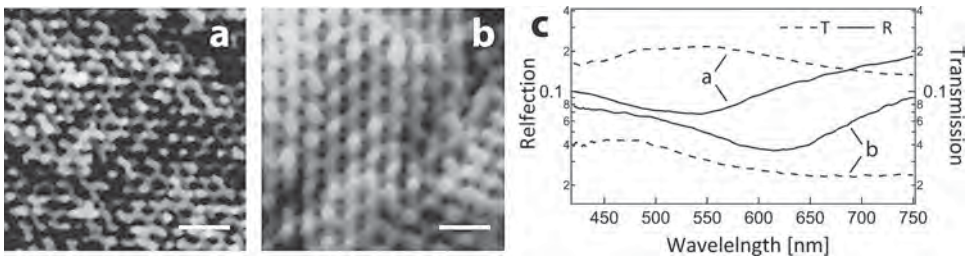

Figure 1. a) SEM images of gold gyroid metamaterials obtained from ISO terpolymers of two different molecular weights, yielding lattice constants of 35 and 50 nm, respectively. b) Spectra of the gold gyroid metamaterials, spectra marked *a* refer to lattice constant of 35 nm, while *b* to 50 nm. Scale bar: 100 nm. c) Corresponding transmission and reflection spectra for unpolarized incident light. Film thickness ≈ 300 nm.

the geometric parameters of the metallic gyroid and the dielectric material it is filled with.

We initially study the influence of the lattice constant *a* on the optical properties by comparing two gyroid morphologies obtained from ISO terpolymers with two different molecular weights but identical block volume fractions (**Figure 1**). The overall molecular weight of the terpolymer directly determines the gyroid unit cell between 10 and ≈200 nm. The used ISO molecular weights of 33 and 53 kg mol^{-1} correspond to measured unit cell sizes of of 35 and 50 nm, respectively, while maintaining the same filling fraction of 30%. The scanning electron microscopy (SEM) images in Figure 1a,b show the gold gyroid structures fabricated from the two ISO terpolymers and Figure 1c compares their reflection and transmission spectra. A remarkable transmission of ≈20% was found for a 300 nm thick layer with the smaller gyroid unit cell. This high transmission across a several-hundred-nanometer-thick layer with Au volume fractions of >30% is evidence for the transport of the optical energy flux through the strut network by plasmon resonances and is therefore the hallmark of an optical metamaterial.

As expected, the highest reflection values are observed on the long wavelength side of the spectrum and a dip in the spectrum is found for both lattice sizes when wave propagation in the gyroid slab is permitted (i.e., for $\lambda < \lambda_p$). Furthermore, as predicted by the THM model, the $a = 50$ nm unit cell has a lower plasma frequency compared to the gyroid with $a = 35$ nm. The reflectivity of the smaller gyroid has a minimum at a wavelength of ≈550 nm, which shifts to ≈620 nm for the larger gyroid. For larger unit cells and identical filling fractions f (i.e., identical effective electron densities) the gyroid struts are thicker and, as a result, the induced self-inductance is stronger, corresponding to a higher effective electron mass per unit cell (see Supporting Information). Since the effective electron mass is linearly proportional to the plasma wavelength, larger lattice constants lead to an increase in the plasma wavelength, as observed in Figure 1c. This property is also clearly evident in Equation 1, where for constant f, λ_p is linearly dependent on a. A smaller value of a however significantly reduces absorption, resulting in transmissions approaching 30% which is remarkably high for a 300 nm-thick gold layer.

The manufactured gyroids can be post-processed by further gold electrodeposition. In the absence of the surrounding polymer matrix, the entire network structure acts as a cathode and gold growth occurs homogeneously to thicken the gyroid struts without affecting the symmetry of the network. This continuously increases the filling fraction by thickening the struts, leaving all other parameters unchanged.

Figure 2 shows the effect of an increase in the filling fraction from 30 to 90%, resulting in a reduction in the plasma wavelength, thereby causing a blue shift of the reflectivity edge to shorter wavelengths. As the filling fraction approaches 100% (i.e., solid gold) the reflection spectra indeed approach that of the gold and the reflection minimum disappears (Figure 2d). As the plasma wavelength defined in Equation 1 cannot easily be extracted from reflection and transmission spectra, we introduce the plasma edge wavelength λ_{pe}, which is the wavelength at the point of inflection of the reflectivity (i.e., the wavelength where the first derivative of the spectrum has a maximum, which is easily identified in experimental and calculated spectra, see Supporting Information for details). Although the plasma edge λ_{pe} and plasma wavelength λ_p are not identical, they have the same behaviour and differ only by small shift as the gyroid metamaterial is tuned.

A quantitative analysis of the results in Figure 2d is shown in **Figure 3**, where the plasma edge wavelength is plotted versus the filling fraction. This analysis reveals a continuous shift in

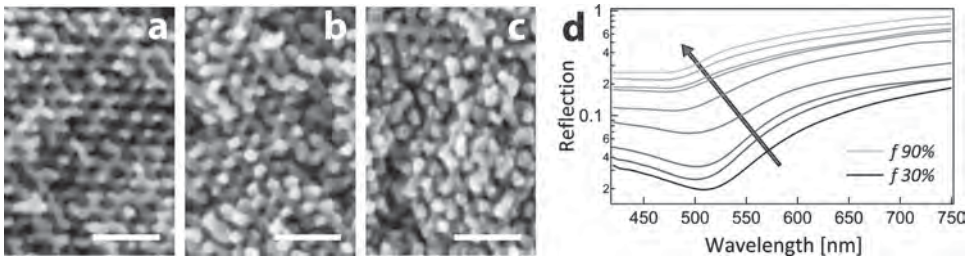

Figure 2. a–c) SEM images of gold gyroids with $a = 35$ nm and filling fractions of 30%, 60%, and 75%, respectively. Scale bar: 100 nm. d) Reflection spectra for filling fractions varying from 30% to 90% in ≈8% increments.

© 2013 WILEY-VCH Verlag GmbH & Co. KGaA, Weinheim
Adv. Mater. **2013**,
DOI: 10.1002/adma.201300193

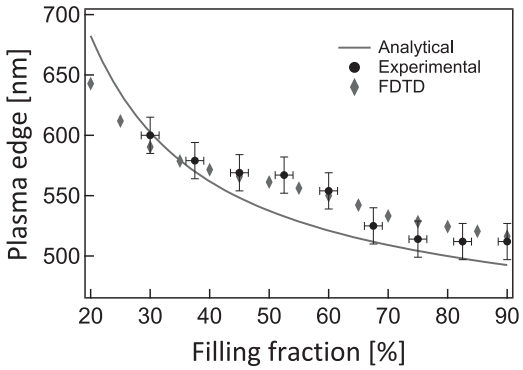

Figure 3. Variation of the plasma edge wavelength λ_{pe} (see Supporting Information, Figure S3) with filling fraction. Experimental data (circles) compared to the THM analytical model (line) and a FDTD calculation (diamonds).

λ_{pe} of more than 100 nm between solid gold and a gyroid with a filling fraction of 30%. These results are in excellent agreement with the results of FDTD calculations (see Supporting Information), as well as with the analytical THM model for the plasma wavelength.

The numerically calculated plasma edge results closely follow the experimental measurements and show only a small divergence from the analytical plasma wavelength. This is due to localized plasmonic modes that are supported on the metallic gyroid, in addition to the three propagating modes (see Supporting Information), which are not taken in account in the analytical model. Due to the complex geometrical shape of the gyroid, multiple localized plasmons are excited, leading to a high density of modes appearing at ≈580 nm and shorter wavelengths for a gyroid with $a = 35$ nm. As the filling fraction increases, the wavelengths at which these high density localized plasmonic modes appear remain relatively constant. The three propagating modes are however shifted to shorter wavelengths until they are fully immersed in the region of the high density of modes. Since the localized plasmonic modes absorb incident fields, they therefore reduce reflectivity and have an impact on the experimentally measured and numerically calculated plasma edge wavelength.

The change of filling fraction also affects the linear dichroism in the [110] direction which is typical for the gyroid metamaterial.[8] **Figure 4** shows the reflection spectra for different filling fractions and with incident polarizations perpendicular and parallel to the in-plane [100] direction of the gyroid lattice. For ≈50% filling fraction, the linear dichroism is lost. The dichroism arises from a variation of the coupling of polarized light with the differing gyroid lattice symmetries. As the anisotropy of the gyroid is reduced with increasing filling fraction, the dichroism disappears.

A further way to reversibly tune the optical response of the gyroid metamaterial involves changing the dielectric medium infiltrated into the gyroid. **Figure 5** shows reflection spectra of the 35 nm unit cell gyroid with a fill fraction of 30% for increasing refractive index media. The plasma wavelength increases linearly with n as illustrated by the variation of the reflectivity curves in Figure 5b. This variation agrees quantitatively with the numerical and analytical results. The modification of the surrounding medium can also be permanently achieved by embedding the gyroid in a polymer matrix or by leaving the polymer scaffold in place after gold deposition.

In conclusion, we have demonstrated three successful approaches to tune the optical behavior of gyroid self-assembled optical metamaterials. Optimised structural parameters led to a transmission through 300 nm thick layers of gyroid-structured gold of up to 20%. These methods can also be applied to other 3D metamaterials. Increasing the lattice dimensions in the gyroid metamaterial reduces the plasma frequency and the transmittivity, which is highest for the small unit cell with the lowest filling fraction. Increasing the gold strut thickness (i.e., the filling fraction) causes a continuous deformation in the shape of the reflectivity curves and increases the plasma frequency towards solid gold. Finally, the optical characteristics can be reversibly tuned by adjusting the refractive index of the medium that is infiltrated into the gyroid pore structure, revealing a linear variation of the plasma edge with n. The robust agreement of the experimental results with model calculations and simulations is highly encouraging, confirming the predictive power of these methods, which now aid in the quest to create a material with a negative refractive index in the visible optical range.

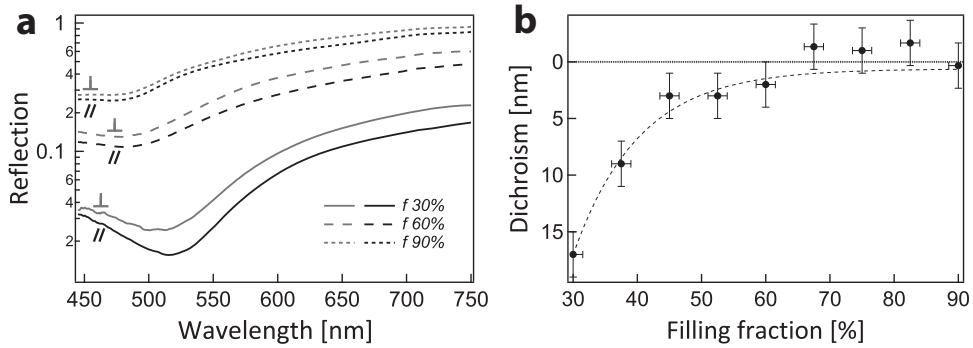

Figure 4. Linear dichroism of the gold gyroid in the [110] direction as a function of the filling fraction. a) Reflection spectra with incident polarization perpendicular (grey) and parallel (black) to the in plane [100] direction of the gyroid lattice. b) Experimental data for the linear dichroism as function of the filling fraction. The dichroism measure was calculated as the difference of the plasma edge wavelengths of perpendicular and parallel polarizations to the [100] direction. The dotted line is a guide to the eye.

© 2013 WILEY-VCH Verlag GmbH & Co. KGaA, Weinheim

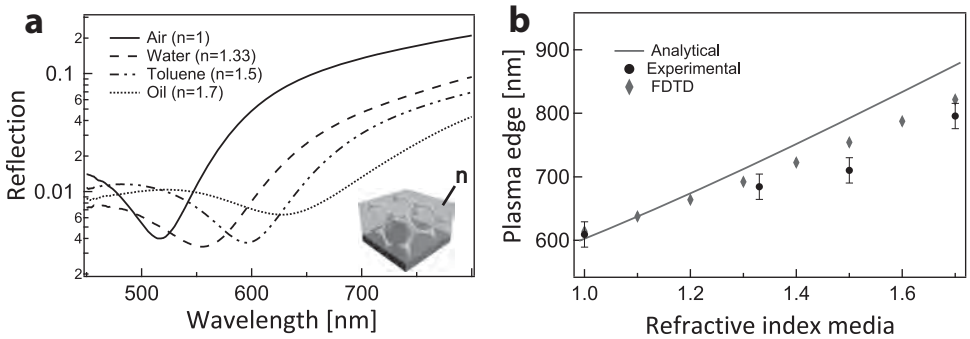

Figure 5. a) Reflection spectra for unpolarized light incident on the $a = 35$ nm gyroid filled with dielectric media: air ($n = 1$), water ($n = 1.33$), toluene ($n = 1.5$), and Cargille Refractive Index Liquid Series B ($n = 1.7$). b) Variation of the plasma edge wavelength λ_{pe} for different refractive index media compared to the THM analytical model and FDTD calculations.

Experimental Section

Sample Preparation: The gyroid forming polyisoprene-*block*-polystyrene-*block*-polyethylene oxide (ISO) triblock terpolymer with relative block volume fractions of 0.28, 0.57, and 0.15 of I, S and O, respectively was used. The synthesis of this polymer is described elsewhere.[19] Several hundred nm-thick films were made by spin-coating followed by annealing for 20 min at 180 °C in a vacuum oven. The isoprene block was then degraded under UV radiation for two hours and rinsed away with ethanol. The resulting porous network was then back-filled with gold by electrodeposition from a glass substrate coated with fluorinated tin oxide (FTO). In the electrochemical setup the FTO layer acts as a working electrode, a saturated calomel electrode is used as the reference electrode, and a platinum mesh acts as the counter electrode. The gold-plating solution was bought from Technin (EC60) and 0.5 vol% of brightener was added to achieve a smooth deposition. The thickness of the deposit could be adjusted by the electrodeposition duration and was set to ≈300 nm. The remaining polymer was subsequently removed by plasma etching (Supporting Information, Figure S1).

Filling Fraction Variation: The filling fraction was varied by further gold electrodeposition on the gold gyroid struts. The resulting gold filling was calculated by measuring the total surface area by oxygen absorption using cyclic voltammetry.[20,21]

Optical Characterization: Confocal optical microscopy was performed using a 50 µm core optical fiber that served as pinhole in the conjugate to the focal plane of a ×20 microscope objective. A broad-band halogen lamp acted as the illumination source. Linear polarization measurements were obtained with a ×100 microscope objective which allowed the collection of a signal with a spatial resolution below the sample domain dimensions. An achromatic polarizer was mounted on a rotational stage to vary polarization rotation. All the measurements were normalized to a silver mirror reference.

Supporting Information

Supporting Information is available from the Wiley Online Library or from the author.

Acknowledgements

The authors thank P. Cunha, M. Scherer and S. Guldin for their invaluable help, and C. Ducati for the high-resolution electron microscopy images in the Supporting Information. We acknowledge the EPSRC EP/G060649/1 for funding.

Received: January 14, 2013
Revised: February 11, 2013
Published online:

[1] C. Rockstuhl, F. Lederer, C. Etrich, T. Pertsch, T. Scharf, *Phys. Rev. Lett.* **2007**, *99*, 017401.
[2] J. F. Galisteo, F. García-Santamaría, D. Golmayo, B. H. Juárez, C. López, E. Palacios, *J. Opt. A: Pure Appl. Opt.* **2005**, *7*, S244–S254.
[3] K. Lodewijks, N. Verellen, W. Van Roy, V. Moshchalkov, G. Borghs, P. Van Dorpe, *Appl. Phys. Lett.* **2011**, *98*, 091101.
[4] V. Saranathan, C. O. Osuji, S. G. J. Mochrie, H. Noh, S. Narayanan, A. Sandy, E. R. Dufresne, R. O. Prum, *Proc. Natl. Acad. Sci. USA* **2010**, *107*, 11676–11681.
[5] K. Hur, Y. Francescato, V. Giannini, S. a. Maier, R. G. Hennig, U. Wiesner, *Angew. Chem.* **2011**, *50*, 12191–12195.
[6] A. Urbas, M. Maldovan, P. DeRege, E. Thomas, *Adv. Mater.* **2002**, *14*, 1850–1853.
[7] H.-Y. Hsueh, H.-Y. Chen, M.-S. She, C.-K. Chen, R.-M. Ho, S. Gwo, H. Hasegawa, E. L. Thomas, *Nano Lett.* **2010**, *10*, 4994–5000.
[8] S. Vignolini, N. a. Yufa, P. S. Cunha, S. Guldin, I. Rushkin, M. Stefik, K. Hur, U. Wiesner, J. J. Baumberg, U. Steiner, *Adv. Mater.* **2012**, *24*, OP23–27.
[9] S. S. Oh, A. Demetriadou, S. Wuestner, O. Hess, *Adv. Mater.* **2013**, *25*, 612–617.
[10] M. Stefik, S. Wang, R. Hovden, H. Sai, M. W. Tat, D. A. Muller, U. Steiner, S. M. Gruner, U. Wiesner, *J. Mater. Chem.* **2012**, *22*, 1078–1087.
[11] A. Minovich, J. Farnell, D. N. Neshev, I. McKerracher, F. Karouta, J. Tian, D. A. Powell, I. V. Shadrivov, H. Hoe Tan, C. Jagadish, Y. S. Kivshar, *Appl. Phys. Lett.* **2012**, *100*, 121113.
[12] A. F. Oskooi, D. Roundy, M. Ibanescu, P. Bermel, J. D. Joannopoulos, S. G. Johnson, *Comput. Phys. Commun.* **2010**, *181*, 687–702.
[13] A. Demetriadou, S. S. Oh, S. Wuestner, O. Hess, *New J. Phys.* **2012**, *14*, 083032.
[14] *Developments in Block Copolymer Science and Technology*, (Ed: I. W. Hamley), John Wiley & Sons, Chichester **2004**.
[15] P. J. Flory, *J. Chem. Phys.* **1942**, *10*, 51–61.
[16] F. S. Bates, G. H. Fredrickson, *Phys. Today* **1999**, *52*, 32–38.
[17] J. Chatterjee, S. Jain, F. S. Bates, *Macromolecules* **2007**, *40*, 2882–2896.
[18] T. S. Bailey, H. D. Pham, F. S. Bates, *Macromolecules* **2001**, *34*, 6994–7008.
[19] S. C. Warren, F. J. Disalvo, U. Wiesner, *Nat. Mater.* **2007**, *6*, 156–161.
[20] M. R. J. Scherer, L. Li, P. M. S. Cunha, O. A. Scherman, U. Steiner, *Adv. Mater.* **2012**, *24*, 1217–21.
[21] S. Trasatti, O. A. Petrii, *Pure Appl. Chem.* **1991**, *63*, 711–734.

© 2013 WILEY-VCH Verlag GmbH & Co. KGaA, Weinheim